Acta mater. 48 (2000) 2823–2835

www.elsevier.com/locate/actamat

MODELLING OF INOCULATION OF METALLIC MELTS: APPLICATION TO GRAIN REFINEMENT OF ALUMINIUM BY Al–Ti–B

A. L. GREER[1]†, A. M. BUNN‡[1], A. TRONCHE[1], P. V. EVANS[2] and D. J. BRISTOW[3]

[1]Department of Materials Science & Metallurgy, University of Cambridge, Pembroke Street, Cambridge CB2 3QZ, UK, [2]Alcan International Ltd, Banbury Laboratory, Banbury OX16 7SP, UK and [3]London & Scandinavian Metallurgical Co. Limited, Fullerton Road, Rotherham S60 1DL, UK

(Received 11 February 2000; accepted 28 March 2000)

Abstract—A numerical model is presented for the prediction of grain size in inoculated castings and is tested against measured grain sizes obtained in standard grain-refiner tests on aluminium alloys. It is shown that for potent nucleants, such as commercial grain refiners for aluminium, the nucleation stage itself is not the controlling factor. The number of grains is determined by a free-growth condition in which a grain grows from a refiner particle at an undercooling inversely proportional to the particle diameter. With measured particle size distributions as input, the model makes quantitatively correct predictions for grain size and its variation with refiner addition level, cooling rate and melt composition. The model can assist in optimizing the use of existing refiners and in developing improved refiners. © *2000 Published by Elsevier Science Ltd on behalf of Acta Metallurgica Inc.*

Keywords: Casting; Aluminium alloys; Nucleation; Kinetics; Grain refinement

1. INTRODUCTION

Grain refinement by inoculation involves addition of particles which can act as substrates for heterogeneous nucleation. Inoculation is particularly widely practised in the aluminium industry [1], both in shaped casting of alloys and in the direct-chill (DC) casting of many wrought grades, including commercial-purity (CP) aluminium. In the latter case, effective grain refinement brings many direct and indirect benefits, including the possibility of faster production rates. There is great interest in the quantitative prediction of solidification microstructure in general and grain size in particular. The grain size depends on, for example, the cooling rate of the melt, its solute level, and the amount of added inoculant. The present work sets out to develop a predictive model for grain size that takes these factors into account. The model is tested against the results of standard grain-refining tests on CP aluminium. The melts have been inoculated with a commercial Al–Ti–B refiner, but the results may be relevant also for other refiners. While the model has been primarily aimed at understanding the grain size in DC-cast billets of aluminium, it should also be applicable for other types of solidification processing and other alloys.

At typical levels of addition of inoculant to aluminium, the grain refinement is very inefficient, with at best 1% of the added particles acting as growth centres for grains. Maxwell and Hellawell [2] suggested that the heating of the melt (*recalescence*) caused by latent heat release from the first crystals to grow would stifle further nucleation events. They assumed that at any time the melt could be taken as spatially isothermal, and they modelled its thermal history taking into account the latent heat release and the external heat extraction. Crystal growth was taken to be initiated by heterogeneous nucleation.

The modelling in the present work is based on that in Ref. [2], but it is shown that heterogeneous nucleation is not necessarily the rate-limiting step for initiation of crystal growth in an inoculated melt. Rather, free growth of a crystal starts on a given particle at an undercooling inversely proportional to the diameter of the particle. For this case, it is essential to assume, more realistically, a distribution of particle size rather than the single size taken by Maxwell and Hellawell [2]. A description of preliminary work on the present model has been given elsewhere [3].

† To whom all correspondence should be addressed.

‡ Present address: Science Museum, Exhibition Road, London SW7 2DD, UK.

1359-6454/00/$20.00
PII: S1359-6454(00)00094-X

2. MECHANISMS OF GRAIN REFINEMENT

2.1. Nucleation mechanism

For grain refinement, the inoculant particles added to the melt must be potent substrates for heterogeneous nucleation. However, the nucleation can occur only if the melt is sufficiently undercooled. In a solidifying system, the remaining melt can be undercooled only if there is some solute in the melt to restrict the growth of the solid, either at a columnar front competing with equiaxed solidification or from particles where nucleation has already occurred. Thus effective refinement requires both heterogeneous nucleation and growth restriction. For the particular case of Al–Ti–B refiners in CP aluminium, prior work on the nucleation mechanism will now be reviewed.

Al–Ti–B refiners consist of TiB_2 particles 0.1 to $\sim$10 μm in diameter and Al_3Ti particles 20–50 μm in diameter, dispersed in an aluminium matrix [4]. Al_3Ti can be a very effective nucleant for aluminium, but this phase dissolves quickly when the refiner is added to CP Al, as the total titanium content in the melt is well within the solubility limit [5]. It is well accepted that some excess titanium (beyond that combined with B in TiB_2) is required for effective nucleation [6]. Recent microscopical studies of refining particles in an Al-rich metallic glass matrix have provided evidence that in the presence of excess Ti, thin Al_3Ti layers can be present on the surface of the TiB_2 particles, even at low overall Ti levels where Al_3Ti would not otherwise be stable [7–11]. The same studies show that c.c.p.-Al nucleates only on the coated {0001} faces of the borides.

The microscopical studies suggest that there is no morphological reason why only $\sim$1% of TiB_2 particles are effective nucleants. A possible speculation is that a small fraction of particles might have surface sites such as ledges particularly favourable for nucleation, but the studies show that such sites are not required. Indeed, re-entrant corners cannot be favoured sites because the c.c.p.-Al forming at such sites avoids contact with the non-{0001} faces of the boride [11]. Neither was any microscopical evidence found for compositional differences between particles giving differences in nucleation performance; Marcantonio and Mondolfo [12], for example, suggested that variations in composition between TiB_2 and AlB_2 (which is isomorphous with TiB_2) could give differences in nucleation.

Studies of solidification of liquid droplets entrained in solid matrices have permitted quantitative analysis of nucleation kinetics. When large undercoolings are required for heterogeneous nucleation ($\Delta T > 50$ K, corresponding to contact angles greater than $\sim 40^\circ$), the classical, spherical-cap model provides a good fit to the kinetics [13], but otherwise the model appears to break down [14]; in the latter case, it has been suggested that an adsorption model may be appropriate [15, 16]. In this model there is a critical undercooling beyond which it is thermodynamically favourable to have an adsorbed layer of a new crystalline phase which is then the basis for growth. Numerous studies have shown that the undercooling for nucleation of c.c.p.-Al by Al–Ti–B inoculants is very small, certainly less than 0.5 K and perhaps as little as 0.01 K (e.g. Refs [17–19]). With such potent nucleation, it seems clear that the spherical-cap model for heterogeneous nucleation cannot be applied. The alternative adsorption model would be consistent with high-resolution transmission electron microscopy observations [10], showing a layer of Al_3Ti as thin as three monolayers on TiB_2 particles in glassy matrix studies.

2.2. Growth restriction

In early work, the degree of growth restriction for a particular solute was described by the *constitutional-supercooling parameter* P [20]

$$P = \frac{m(k-1)C_0}{k} \tag{1}$$

where m is the liquidus slope, k is the equilibrium partition coefficient, and C_0 is the solute content in the alloy melt. In the absence of solute interactions, the overall constitutional-supercooling parameter for a multicomponent alloy can be estimated by summing the P values for each element [21, 22].

Maxwell and Hellawell [2] considered growth of spherical crystals restricted by the partitioning of a single solute. To a good approximation the crystal growth rate for a given undercooling is proportional to the diffusivity of the solute in the liquid and inversely proportional to the parameter Q ($\equiv 1/X$ in Ref. [2])

$$Q = m(k-1)C_0 = kP. \tag{2}$$

In the present work Q is termed the *growth-restriction parameter*. Desnain *et al.* [23] extended the Maxwell–Hellawell treatment to multicomponent alloys and showed that for these, the overall growth-restriction parameter is again the sum of the Q values for the individual solutes. Hodaj and Durand [24] introduced a new growth-restriction parameter U in which the contributions of the various solutes are weighted inversely by diffusivities. However, reliable values for solute diffusivities in liquid aluminium are difficult to obtain. In the present work, we assume that all the solute diffusivities are essentially the same, and quantify the growth restriction by summing Q values.

A major study of solute effects by Spittle and Sadli [25] used inoculated binary alloy melts with a wide range of solute types and amounts to show that there appears to be a universal curve relating grain size to P. As P is increased, the grain size at

first decreases sharply, and then levels off when $P \geq 15$ K. It will be shown (Section 5.4) that the experimental data of Spittle and Sadli are better interpreted in terms of Q.

2.3. Analysis by Maxwell and Hellawell

The basis of the Maxwell–Hellawell model [2] is that restriction of the growth of already nucleated grains permits continuing nucleation in the undercooled melt until the total latent heat release is sufficient to cause recalescence and the loss of undercooling. Classical steady state nucleation theory was applied to calculate the rate of formation of spherical-cap nuclei on refiner particles. It was assumed that once formed a nucleus would quickly envelop a particle, giving one nucleation event per particle. The nucleation rate on a particle is dependent on the undercooling, the contact angle θ, and the particle size. In the calculations only single values of θ and particle size were used. While Maxwell and Hellawell recognized the limitations of the spherical-cap model, they took θ to be a convenient measure of nucleation potency. The growth of the grains was taken to be spherical and restricted by the curvature undercooling and by solute diffusion.

The release of latent heat was calculated and the competition with external heat extraction led to cooling behaviour (modelled numerically) in which undercooling is followed by recalescence and a thermal plateau. The value of the limiting grain size at high refiner additions was studied as a function of the key parameters. Lower θ (more potent nucleants) and higher cooling rate give a finer limiting grain size. Increased growth restriction [quantified as Q in equation (2)] has a strong effect in reducing the limiting grain size. Only self-inoculating binary peritectic systems (Al–Ti, Al–Zr, Al–Cr) were considered, however. Increased nucleant particle size had only a weak effect in reducing the limiting grain size. Maxwell and Hellawell did not undertake a quantitative experimental test of any of these predictions.

3. EXPERIMENTAL

The grain refiner used was Al–5Ti–1B (wt%), as supplied commercially in 9.7 mm diameter rod form by London & Scandinavian Metallurgical Co. Limited. The microstructure of the refiner itself was studied by scanning electron microscopy (SEM) of polished sections. With backscattered electron imaging, the TiB_2 particles appear bright against the darker matrix, with sufficient contrast to permit image analysis to determine their size distribution.

Grain-refining tests were carried out on commercial-purity (CP) Al, using the Aluminum Association TP-1 test [26], with an addition level of one part per thousand (p.p.t.) by weight (equivalent to 1 kg of rod added per tonne of molten aluminium), unless specified otherwise. Samples were taken for grain-refining tests after selected times, mostly after 2 min. In each case the melt was maintained at 718 ± 5°C, and was stirred thoroughly before each sample was taken. Stirring is known to prevent *fading* (increase of grain size with the time that the refiner particles have been present in the melt before cooling) which can be attributed to particle settling [27, 28]. Test samples are removed from the metal bath in a conical steel ladle, which is then lowered into a retaining ring and quenched from below until solidification is complete. The cooling rate at the section height (see below) in the standard TP-1 test was estimated by direct measurement in sample tests to be 3.5°C/s. This is within the expected range for the TP-1 test, which is intended to duplicate the cooling rate found in DC-cast ingots.

Each cone is then sectioned perpendicular to its axis 38 mm from its base, polished to remove any scratches and then etched in Poulton's reagent to highlight the grain boundaries. The mean linear intercept, $\bar{l}$, was then estimated by counting the number of grain-boundary intercepts along two perpendicular 13 mm long lines, randomly placed in the central area of the etched surface. No correction was made for the potential omission of intercepts by over-etching of small grains; the measurements may therefore somewhat overestimate the grain size. The error in the grain-diameter determination is estimated to be ± 20 μm.

All grain diameters quoted are values of mean linear intercept $\bar{l}$. The numerical model calculates the number of grains per unit volume N_V. In comparing experimental measurements with model predictions, the values of N_V and $\bar{l}$ are interconverted using

$$N_V = \frac{0.5}{\bar{l}^3} \tag{3}$$

(see Appendix).

Apart from the TP-1 tests, cooling curves were determined for melts cooled in alumina crucibles. To vary the cooling rate the crucible was set on a copper chill block (1 K/s), allowed to air-cool (0.75 K/s) or wrapped in an insulating blanket (0.5 K/s).

4. FREE-GROWTH MODEL

4.1. Nature of the growth onset

The TiB_2 particles in the refiner are faceted hexagonal platelets with large {0001} faces on which nucleation occurs; in the present work these are treated as discs of diameter d. It is assumed that a nucleus is formed on the face of a particle at very

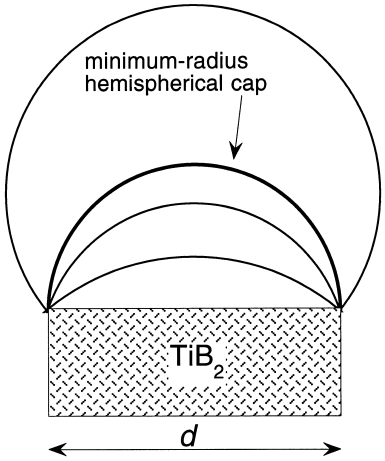

Fig. 1. Crystal growth following nucleation (by the classical heterogeneous mechanism, or by adsorption) on one {0001} face of a boride particle. Thickening of the crystal reduces the radius of curvature of its interface with the liquid. As this radius cannot go below the critical nucleus radius r^*, there is a barrier to free growth if $d < 2r^*$. Further growth past the critical hemispherical condition (for which the solid–liquid interface has minimum radius of curvature) is then possible only by increasing the undercooling to reduce r^*.

low undercooling, whether as a low-contact-angle spherical cap or by adsorption. Initially, the newly formed crystal can grow laterally, but when it completely covers the face of the boride it can grow further only by reducing the radius of curvature of its interface with the melt (Fig. 1). This radius cannot go below the critical value r^* for nucleation at the instantaneous temperature. If the diameter of the particle is such that $d < 2r^*$, then *free growth* of the crystal from the particle is not possible. It becomes possible only at greater undercooling when r^* is reduced. The critical condition for free growth of the crystal through the minimum-radius hemispherical shape is when $d = 2r^*$. The undercooling for free growth ΔT_{fg} and the nucleant particle diameter d are simply related by

$$\Delta T_{fg} = \frac{4\sigma}{\Delta S_V d} \tag{4}$$

where σ is the solid–liquid interfacial energy and ΔS_V is the entropy of fusion per unit volume. Undercooling experiments give lower-bound estimates of σ [29]. We take the highest available value of $\sigma = 158\ \mathrm{mJ/m^2}$ from contact-angle measurements [30]. With ΔS_V as in Table 1, TiB_2 particles in the refiners, 0.1–10 μm in diameter, would give ΔT_{fg} in the range 5.7 K down to 0.06 K. This range spans the values quoted for nucleation undercooling, suggesting that the free-growth barrier is dominant. The condition for free growth is not significantly affected by whether the crystal "wets" some or all of the faces of the particle. In the present work it is assumed that each nucleant particle can be a growth centre for at most one grain.

Since the onset of growth is controlled by the growth constraint rather than by nucleation, it is not stochastic. As the undercooling is increased, progressively smaller particles become centres for free growth, which occurs as soon as the required undercooling is reached, without any delay such as would be associated with a finite nucleation rate. In the modelling (assuming an isothermal melt), this has the important consequence that a single particle diameter would lead to growth of grains starting simultaneously on all particles. This unrealistic outcome is avoided by modelling with a distribution of particle diameter. It is in any case known (Sections 2.1 and 5.1) that the particles in actual refiners do show a substantial size distribution.

4.2. Isothermal melt

The essence of the present model is that the growth of some grains must stifle further nucleation, thus limiting the efficiency of the refiner. There are three ways in which stifling of further nucleation events could occur: (i) by hard impingement of the growing grains, (ii) by soft impingement of the solute diffusion fields around the growing grains, or (iii) by soft impingement of the thermal diffusion fields. Maxwell and Hellawell [2] showed that (iii) is clearly dominant; this is basically because in the melt the thermal diffusion coefficient is four orders of magnitude greater than the solute diffusion coefficient.

In an alloy in which there is a clear refinement effect, the average grain diameter, and therefore the approximate separation between active growth centres, can be as much as 200 μm. The solutal diffusion length is much less than this range. For typical solidification velocities, the thermal diffusion length is two to three orders of magnitude greater

Table 1. Parameters used in the calculations. The material parameters are mostly for pure aluminium

Quantity	Symbol	Units	Value	Reference
Solid–liquid interfacial energy	σ	$\mathrm{mJ/m^2}$	158	[30]
Entropy of fusion per unit volume	ΔS_V	$\mathrm{J/K\ m^3}$	1.112×10^6	[31]
Enthalpy of fusion per unit volume	ΔH_V	$\mathrm{J/m^3}$	9.5×10^8	[31]
Heat capacity of melt per unit volume	C_{pV}	$\mathrm{J/K\ m^3}$	2.58×10^6	[32]
Diffusivity in melt (Ti in Al)	D_s	$\mathrm{m^2/s}$	2.52×10^{-9}	[33]
Cooling rate in TP-1 test	$\mathrm{d}T/\mathrm{d}t$	K/s	3.5	[26] and this work

than this range, showing that the assumption of an isothermal melt is well founded.

As the melt is cooled below the liquidus temperature, free growth of crystals occurs first on the largest inoculant particles, and then on more, smaller particles. All the growing crystals release latent heat that is distributed uniformly through the melt, slowing the rate of cooling, and eventually causing the temperature to rise (recalescence). After the temperature has started to rise, there is no further initiation of free growth. Thus recalescence limits the refinement of grain size. Quantitative predictions require computation of the crystal growth rate, which is considered next.

4.3. Crystal growth

In the operating conditions of slow growth in a near-isothermal melt, only the curvature and solutal undercoolings are significant. For a spherical crystal of radius r, the curvature undercooling ΔT_c is given by

$$\Delta T_c = \frac{2\sigma}{\Delta S_V r}. \tag{5}$$

The solutal undercooling ΔT_s is given by

$$\Delta T_s = m(C_0 - C_{IL}) \tag{6}$$

where m and C_0 are as already defined, and C_{IL} is the solute content in the melt at the solid–liquid interface.

The present model calculates the crystal growth rate according to the method of Maxwell and Hellawell [2], briefly outlined here. The growth in the relevant, early stages can be taken to be spherical and not dendritic. In an isothermal melt, the radius r of a growing spherical crystal is given by [34]

$$r = \lambda_s (D_s t)^{1/2} \tag{7}$$

where D_s is the solute diffusion coefficient in the liquid and t is the time. The parameter λ_s is obtained using the invariant-size approximation [34]

$$\lambda_s = \left(\frac{-S}{2\pi^{1/2}}\right) + \left(\frac{S^2}{4\pi} - S\right)^{1/2}. \tag{8}$$

Here S is given by

$$S = \frac{2(C_{IL} - C_0)}{(C_{IS} - C_{IL})} \tag{9}$$

where C_{IS} is the solute content in the solid at the solid–liquid interface. As illustrated in Ref. [2], S can vary between 0 and -2. In the present case, in which the overall melt undercooling $\Delta T = \Delta T_s + \Delta T_c$, S is given by

$$S = \frac{2\left[\dfrac{\Delta T - \Delta T_c}{m}\right]}{(k-1)\left(\left[\dfrac{\Delta T - \Delta T_c}{m}\right] + C_0\right)}. \tag{10}$$

Differentiating equation (7) with respect to time, and rearranging, gives the growth rate of a spherical crystal as

$$V = \frac{dr}{dt} = \frac{\lambda_s^2 D_s}{2r}. \tag{11}$$

Thus the instantaneous growth rate of a spherical crystal depends on the overall undercooling ΔT, the crystal radius r and alloy composition C_0, in addition to the alloy parameters m, k, σ, ΔS_V and D_s.

4.4. Numerical calculation

The calculations are performed for a notional $1\ m^3$ of melt. The thermal history of the melt is treated as a series of short temporally isothermal steps of duration dt. In the absence of solidification

$$T_{n+1} = T_n - R\,dt \tag{12}$$

where T_n is the temperature of the (spatially isothermal) melt in the nth time interval, and R is the imposed cooling rate. The inoculant particles are classified into bins by diameter d, the number of particles in the range d to $d + \delta d$ being $N(d)\delta d$. For each such set of particles, crystal growth on them is initiated when the melt undercooling (measured relative to the liquidus) reaches, or exceeds, their free-growth undercooling [equation (4)]. In all subsequent time intervals, the radius of the crystals growing on this set of particles is changed according to

$$r_{n+1} = r_n + V\,dt \tag{13}$$

where V in the nth interval is calculated using equation (11), but with the value of r taken to be that in the $(n-1)$th interval; this ensures that growth can occur as soon as ΔT_{fg} is reached.

For the set of crystals growing on the particles of diameter d to $d + \delta d$, there is a heat input $q(d)\delta d$ into the melt in the nth time increment:

$$(q(d)\delta d)_n = N(d)\delta d\, 4\pi r_{n-1}^2 (r_n - r_{n-1})\Delta H_V \tag{14}$$

where ΔH_V is the latent heat of solidification per unit volume. In every time increment, the heat inputs from each set of growing crystals are summed to obtain the total q_{total}, and the melt temperature in the next interval is then given by

$$T_{n+1} = T_n - R\,dt + \frac{q_{total}}{C_{pV}} \tag{15}$$

where C_{pV} is the specific heat of the melt per unit volume. There is no need to change the specific

heat according the fraction solidified, because that fraction is so small in the range of interest.

In applying the model (implemented in FORTRAN 77), the initial time interval was reduced only to the stage where further reduction led to a change in the computed grain size of less than 1%. It was found that a suitable starting interval is $dt = 10^{-4}$ s. This interval was reduced as the calculation progressed, roughly in proportion to the magnitude of the instantaneous rate of change of temperature.

In applying equation (13) in each time interval, the approximation is made that the solute profile around a growing grain at any instant has the same form as that for a grain of the same size which had grown isothermally at the instantaneous temperature.

4.5. Spherical growth

Before presenting the results (Section 5), it is important to verify that the operation of the numerical calculation is consistent with the assumptions made in formulating the model. Spherical crystal growth has been assumed, but a dendritic morphology is expected after the very early stages of growth. The onset of the cellular/dendritic instability has been analysed by Mullins and Sekerka [35]. They showed that spherical growth would be absolutely stable for crystal radii less than approximately seven times the critical radius for nucleation under the same conditions. Relative stability (in which a perturbation on the spherical shape grows no faster than the sphere itself) applies for radii less than ~ 21 times the critical radius for nucleation. Figure 2 shows that, even for the largest crystals arising in the numerical modelling, the assumption of spherical growth seems justified for the early stages of solidification which are relevant for recalescence and analysis of grain refinement.

5. TESTING THE MODEL

5.1. Parameters in the model

Table 1 shows the parameters used. The materials parameters are taken to have the values for pure aluminium, even though in principle the values would be affected by alloying. The relevant solute diffusivity is taken to be that of titanium in the aluminium melt near the melting temperature. In effect it is assumed that other solutes have similar D_s values.

The full composition of the CP aluminium used in the present experiments has been given in Ref. [28]. Table 2 shows only those solutes present in sufficient quantity to make a significant contribution to the growth restriction. When Q is used to represent the growth restriction, titanium is clearly the dominant solute. The model for solute-controlled growth (Section 4.3) is for one solute only. In applying the model to CP aluminium, the alloy has been taken to be binary Al–Ti with Ti content to match the overall Q value. Thus the CP aluminium with total $Q = 1.37$ K has been modelled as Al–0.009 wt% Ti, which would have the same Q. The exact composition of Al–5Ti–1B (wt%) refiner used has been given in Ref. [28]. At the addition levels used (up to 10 p.p.t.), the refiner changes the composition of the melt to which it is added only by increasing the Ti content. The effect of the extra Ti—the overall Q increases by 0.42 K for each 1 p.p.t. addition—is significant and must be taken into account in the modelling.

Image analysis of the refiner was used to obtain a

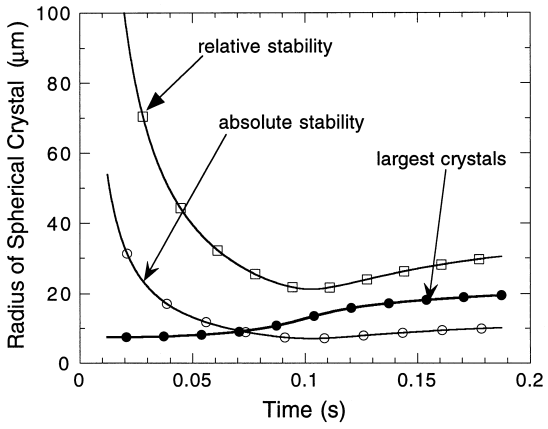

Fig. 2. Predictions of the model for CP aluminium inoculated with 2 p.p.t. of Al–Ti–B refiner and cooled at 3.5 K/s. For the largest (first freely growing) grains, their radius is compared with the radii for absolute and relative morphological instability [35]. At the relevant early stages of solidification, spherical crystal growth can be assumed.

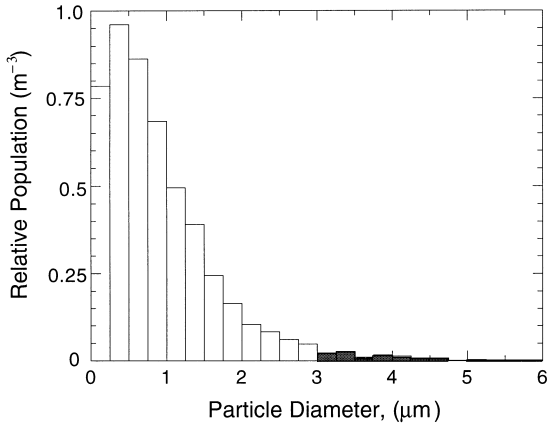

Fig. 3. The shape of the TiB_2 particle diameter distribution in Al–5Ti–1B (wt%) refiner, as determined from image analysis of scanning electron micrographs. The total number of particles in the diameter range 0.2–6.0 μm is calculated (from the volume fraction of TiB_2) to be $\sim 5 \times 10^{13}/m^3$. The dark shaded portion shows those particles likely to be active under typical conditions.

Table 2. The values of m (liquidus slope), k (equilibrium partition coefficient), C_0 (solute content), constitutional-supercooling parameter P [from equation (1)] and growth-restriction parameter Q [from equation (2)] for the solutes of interest in the commercial-purity aluminium used in the present work. The m and k values are calculated from parameters in Ref. [36]. The composition of the commercial-purity Al is also discussed in Ref. [28]. Of the solutes present in CP aluminium, only those contributing > 0.1 K to the overall P or > 0.01 K to the overall Q are given. The addition of refiner increases the dissolved titanium content in the melt; the value given is for an addition of 1 p.p.t. (by wt)

Solute element	m (K/wt%)	k	C_0 (wt%)	P (K)	Q (K)
Fe	−2.925	0.03	0.0825	7.8	0.234
Si	−6.62	0.12	0.0475	2.3	0.276
Ga	−2.52	0.14	0.0125	0.2	0.028
Ni	−3.50	0.004	0.0051	4.4	0.018
V	9.71	3.33	0.0079	0.05	0.167
Ti	25.63	7	0.0042	0.09	0.63
Na	−7.84	0.013	0.0015	0.9	0.012
Totals for CP Al				15.74	1.37
Ti (from 1 p.p.t. addition of refiner)	25.63	7	0.0028	0.06	0.42

population distribution of the longest particle dimension for TiB_2. The total number of particles measured for obtaining a distribution was of the order of 5000. Standard stereological methods [37] were applied to convert the length distribution as measured on a two-dimensional section into the true three-dimensional distribution of disc diameter, shown in Fig. 3. At low particle sizes the populations become uncertain, as scratches and other blemishes on the sections may be wrongly interpreted in the image analysis. This is not a major problem as the grain refinement performance is dominated by the largest particles. Particles below 0.2 μm in diameter and above 6.0 μm were barely detectable, and in the modelling the diameter distribution is considered only between these limits. Within the range considered, and especially for diameters > 1 μm, the population distribution can be well fitted by an exponential form:

$$y = y_0 \exp\left(-\frac{d}{d_0}\right) \tag{16}$$

where d is the particle disc diameter and d_0 is the characteristic width of the distribution. For the results in Fig. 3, fitting the diameter range 1–6 μm, the best-fit value of d_0 is 0.72 μm.

Having obtained the shape of the particle diameter distribution by metallographic examination, it was more accurate to obtain the absolute numbers of particles from the composition of the refiner. Several transmission electron microscopy studies (associated with the work in Refs [7–11]) showed that the TiB_2 particles are hexagonal platelets with thickness ~35% of their diameter. In the calculation, these were approximated as discs of the same aspect ratio. For 1 wt% B in the refiner, the total volume fraction of TiB_2 is 2×10^{-5}, and this was taken to be the integral of particle volume over the diameter range. In this way, the absolute particle populations were estimated. The calculation is not sensitive to the value taken for the upper limit of particle diameter, provided this is large enough, > 5 μm.

5.2. *Addition level of refiner*

It is well known that inoculation of melts becomes less efficient as addition levels are raised. The near saturation of the grain refinement at high addition levels was confirmed experimentally in a series of TP-1 tests. Figure 4 shows that the grain diameter is strongly dependent on addition level only for additions less than ~1 p.p.t., and saturates at 130 ± 20 μm for high additions.

The model was used, taking the parameters from various sources in Table 1 and the particle-diameter distribution, without adjustment. It successfully reproduces the basic form of the grain size variation. At high addition levels, the model predicts a grain diameter of ~90 μm, continuing to decrease slowly with increasing addition. The similarity between experiment and prediction strongly supports the validity of the model, in particular the conjecture that the efficiency of the inoculation is limited by recalescence.

The measured and predicted data in Fig. 4 are

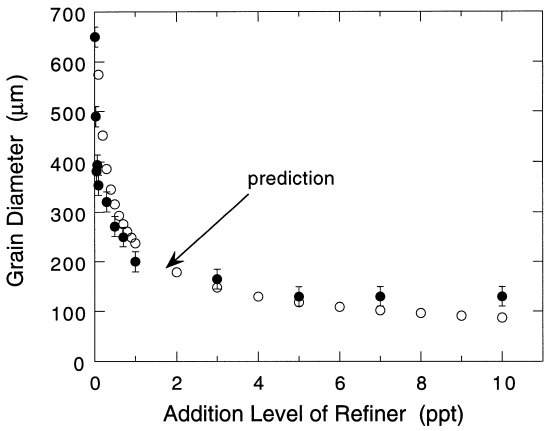

Fig. 4. Grain size (mean linear intercept) for CP Al inoculated with Al–5Ti–1B at various levels. The grain diameters measured in TP-1 tests (●) are compared with the model predictions (○) assuming a cooling rate of 3.5 K/s. Good agreement is found, even though the model has no adjustable parameters.

replotted in Fig. 5, which makes clearer the refiner efficiency (the ratio of the number of grains to the number of added refiner particles). Again it is seen that the model successfully predicts the general form of the observed behaviour. Also shown in Fig. 5 is the prediction of Maxwell and Hellawell [2], who found two regimes: (a) in which the efficiency is 100%, and (b) in which the grain size is essentially constant. The present results, in contrast, do not approach efficiencies of 100%, and do not show a sharp transition between two regimes. The key difference between the models is in the distribution of inoculant particle characteristics. Maxwell and Hellawell made calculations only for particles with uniform characteristics (contact angle and size). Grain nucleation occurs stochastically on the particles and thus is spread over a range of undercooling. However, if a given temperature was maintained long enough, nucleation would eventually occur on all the nucleant particles; in this way 100% efficiency would be achieved. With the present model, however, the distribution of particle diameters means that at any undercooling, only a fraction of the particles could ever be active growth centres. The exponential nature of the measured diameter distribution (Fig. 3) shows that a large fraction of the particles may never reach the undercooling at which they would become active. An efficiency of 100% is then impossible.

5.3. Cooling rate

In solidification in general, including that of inoculated melts, faster cooling gives a finer grain size. To quantify this effect, CP-Al melts were cooled at various rates. In addition to the standard TP-1 test (~ 3.5 K/s) and a modified TP-1 test with increased quenching (~ 5.5 K/s), melts were cooled in alumina crucibles at various rates as described in Section 3. In each case, the cooling rate just before the onset of freezing was measured using a thermocouple embedded in the melt. The results are shown in Fig. 6 and compared with the model predictions. Despite the limited number of measurements, it can be concluded that there is some consistency between experiment and prediction. As shown by the model, there is a strong variation of grain size at low cooling rate, tending to saturate at high cooling rate. Typical grain-refining tests are in a regime where the grain size could be significantly affected by the cooling rate.

5.4. Growth restriction

The data of Spittle and Sadli [25] from an extensive series of grain-refining tests are reproduced in Fig. 7. To facilitate the interpretation of solute effects, these tests used high-purity aluminium with carefully controlled solute additions. The data are plotted as a function of the growth-restriction parameter Q, rather than P as in the original work. The scatter of the data about the trend line can be estimated as an r.m.s. deviation in grain diameter, and this was calculated for grain diameters less than 400 μm (for which the grain structures are expected to be refined and equiaxed, as discussed in the next paragraph). The r.m.s. deviation of grain diameter is estimated to be 45 μm for the plot in Fig. 7, slightly smaller than the value of 51 μm obtained for the original P-plot in Ref. [25]. This

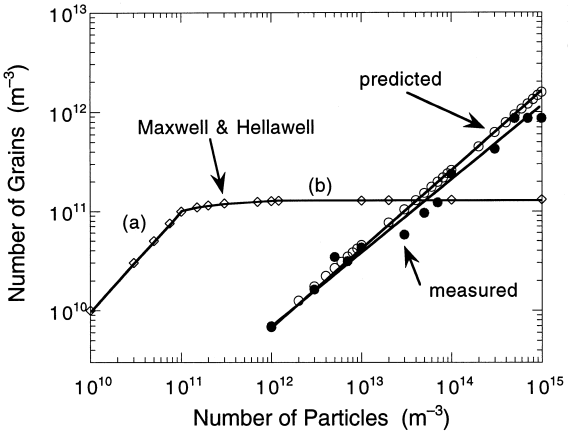

Fig. 5. The number of grains per unit volume as a function of the number of refiner particles per unit volume, showing a general trend to lower efficiency at higher addition level. Data calculated from grain diameters measured in TP-1 tests (●) are compared with predictions of the present model (○). Also shown are the predictions of Maxwell and Hellawell [2]. Assuming nucleation on a set of particles with fixed characteristics, they find two regimes: (a) in which there is 100% efficiency (one grain per particle), and (b) in which the number of grains saturates.

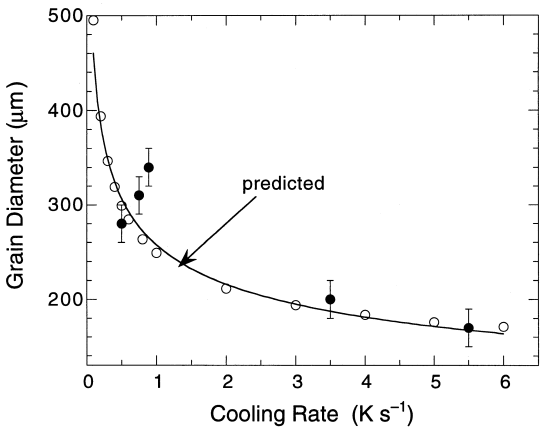

Fig. 6. The grain size of CP Al with 5 p.p.t. addition of Al–5Ti–1B as a function of cooling rate, measured (●) in a TP-1 test ($dT/dt = 3.5$ K/s for standard test and 5.5 K/s with increased quenching) and in other tests in alumina crucibles (Section 3), and compared with model predictions (○).

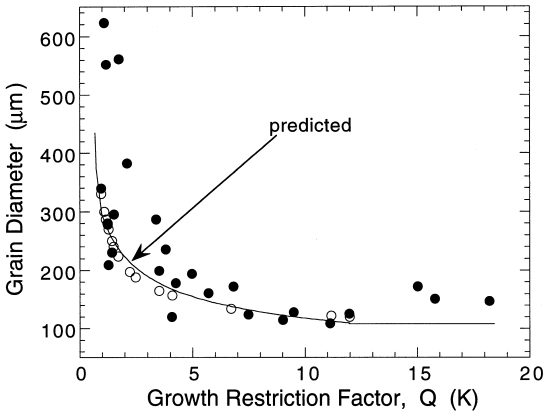

Fig. 7. Grain size as a function of growth-restriction parameter Q [equation (2)] for a standard TP-1 test with 2 p.p.t. addition of Al–5Ti–1B refiner. The measured data (●) from Spittle and Sadli [25] are compared with predictions (○) from the model, taking parameters appropriate for each chosen solute.

may suggest that Q is a better parameter than P for quantifying the degree of growth restriction.

For each of the solutes (Cr, Cu, Fe, Mg, Mn, Si, Zn and Zr in various amounts), the appropriate m and k values were put into the model. The solute contents were adjusted to take account of the Ti in the melt arising from the 2 p.p.t. refiner addition used by Spittle and Sadli. The standard particle-diameter distribution was used, with other parameter values as in Table 1. As shown in Fig. 7 and also in Fig. 8, the model predictions match the experiment well, especially at the important refined grain sizes of less than 400 μm. For larger grain sizes (at low values of Q), it is probable that the grain structures in the tests were columnar, in which case the present model does not apply.

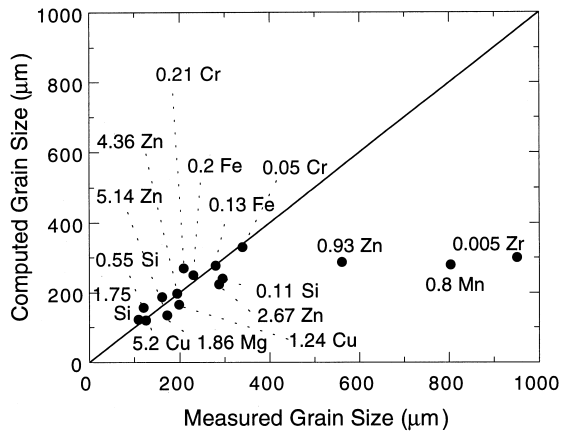

Fig. 8. Comparison of measured data (as in Fig. 7, from TP-1 tests [25]) with the grain diameters computed using the present model. In the computations, the various solute contents (shown in wt%) were taken into account, together with the Ti solute from the added refiner (2 p.p.t. of Al–5Ti–1B).

P characterizes the largest growth restriction which could be achieved for a given composition, and corresponds to the maximum solutal undercooling, relevant for steady state growth of a planar front. In contrast, Q characterizes the degree of growth restriction for a small undercooling set independently. The measured grain sizes do appear to conform better to a correlation based on Q. This suggests that the growth restriction controlling the effectiveness of inoculation is that at a small undercooling, and not that at the maximum possible undercooling.

Certainly, Q is central in the Maxwell–Hellawell model as adapted here. From a Scheil analysis, the derivative of solid fraction with temperature at the onset of solidification is found to be $1/Q$. Thus higher Q implies a slower onset of solidification, slower latent heat release, deeper undercooling before recalescence and therefore initiation of free growth on more particles.

Despite some earlier modelling work [38], there appears to have been no previous attempt to explain quantitatively the shape of the curve in Fig. 7. The agreement between measured and predicted grain diameters evident in Figs 7 and 8, justifies the solute diffusion analysis in the Maxwell–Hellawell model and in the present model. The limited scatter of the experimental data in these figures is evidence that taking D_s as a constant is a reasonable approximation.

5.5. *Cooling curves*

Measured cooling curves have long been correlated empirically with microstructure development

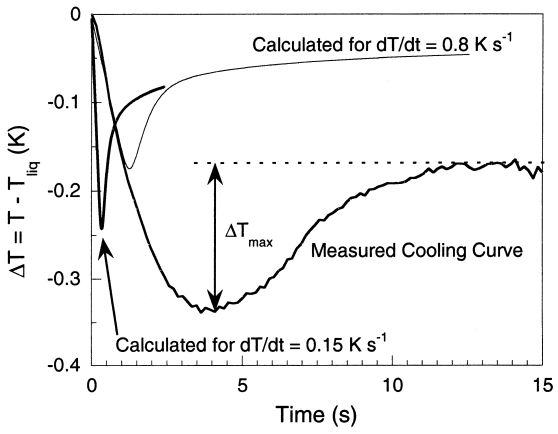

Fig. 9. Measured and calculated cooling curves for an Al–0.5 wt% Fe sample with 5 p.p.t. added refiner cooled at 0.8 K/s in an alumina crucible in air. As the measured temperatures are subject to zero-point error, the maximum undercooling ΔT_{max} is estimated on the experimental curve relative to the thermal plateau following recalescence. The measured cooling rate at the liquidus temperature is 0.15 K/s and calculated curves are shown both for 0.8 and 0.15 K/s.

in castings and they have been used in studies of grain refinement [4]. Since the present model is based on recalescence limiting the number of grains, it is of particular interest to compare measured cooling curves with model predictions. Since the expected undercoolings are so small, it is necessary to measure the temperature with care. The absolute temperature is difficult to calibrate with sufficient accuracy, so the maximum undercooling ΔT_{max} is measured relative to the thermal plateau after recalescence, as shown in Fig. 9. Since the plateau temperature is affected by changing curvature and solutal undercoolings, this estimation can only be approximate. Cooling curves were measured in a series of tests on Al–0.5 wt% Fe (varying cooling rate and refiner addition level) on melts in alumina crucibles; all showed recalescence, agreeing with the basic feature of the model. The measured curves show that the cooling rate decreases significantly as the liquidus temperature is approached. In the example in Fig. 9 (cooling in air), the cooling rate of 0.8 K/s has decreased to 0.15 K/s at the liquidus temperature itself. In the figure, the measured cooling curve is compared with curves calculated both for 0.8 K/s and for the apparent local cooling rate of 0.15 K/s. In all cases, ΔT_{max} is $\sim$0.2 K, the good agreement supporting the concept that the number of grains is indeed limited by recalescence. The measured time to recalescence is, however, significantly greater than that predicted by the model, even for the lower cooling rate. This discrepancy, and the low measured cooling rate at the liquidus temperature, may arise largely because the melt in the test is not perfectly isothermal as assumed in the modelling. In the test sample, solidification progresses through the melt and is more spread in time than in the model. Further aspects of the solidification being non-isothermal are considered in Section 7.

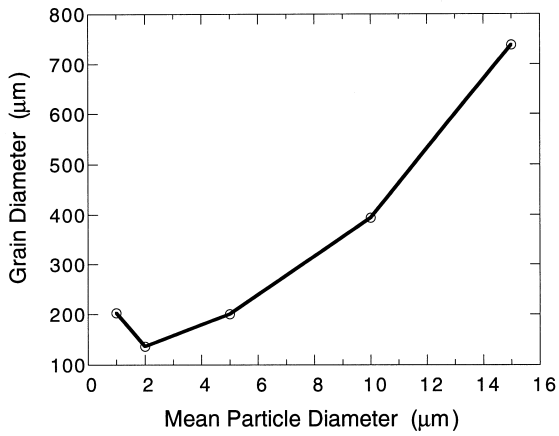

Fig. 10. Refinement of CP Al with 1 p.p.t. addition of Al–5Ti–1B refiner. The predicted grain size as a function of average inoculant particle diameter is shown for an assumed Gaussian distribution of particle diameter with width (standard deviation) of 0.5 μm.

The number of freely growing grains increases steadily during cooling until the minimum temperature is reached at the point of recalescence. As the temperature starts to rise, some of the smallest new grains redissolve (illustrated in Ref. [3]). The number redissolving is negligible, however, compared with the total; to a very good approximation, the final number of grains is the number of initiation events before recalescence.

6. DESIGNING A BETTER REFINER

The model suggests that if the particle-diameter distribution could be restricted to the shaded portion in Fig. 3, the refiner would show 100% efficiency. Such a size distribution is not likely to be achievable, however. A thorough consideration of how the modelling could direct refiner design is beyond the present scope, and is considered elsewhere [39]; preliminary results are shown in Fig. 10. Here, for a 2 p.p.t. addition of Al–5Ti–1B, it has been assumed that the TiB_2 particles have a Gaussian diameter distribution; the width (standard deviation) of this distribution has been taken to be 0.5 μm. Figure 10 shows that the grain size shows a minimum as average particle diameter is decreased. The form of this curve is not very sensitive to the width of the distribution, and it reflects competing trends. As the average particle diameter is decreased (at constant volume fraction), the number of particles must increase, and this leads to a decrease in grain size, though this effect is likely to saturate, as suggested by the form of Fig. 4. Smaller particles give intrinsically less good refinement as their activation at greater undercooling leads to faster growth. (It is found, though not illustrated here, that smaller average particle diameter gives larger grain size if the number of particles is held constant.) Overall, then, there appears to be an optimum average particle diameter, in this case of $\sim$2 μm. Other effects are discussed more fully in Ref. [39].

7. DISCUSSION

Settling of inoculant particles is not accounted for in the model. Although settling appears to be negligible in the stirred melts used in the present experimental studies, this would not always be the case. Similarly, particle agglomeration may have to be taken into account for accurate modelling in some cases.

In general, as seen in Figs 4–8, there is good agreement between predicted and measured grain sizes. The success of the model implies that the Al–5Ti–1B refiner is in most cases essentially a perfect nucleant. The model, based on the free-growth barrier [equation (4)], then correctly gives the funda-

mental limit to possible refinement. However, if there is a significant nucleation barrier, the model does not apply.

For example, the presence of some solutes in the melt can dramatically reduce refiner effectiveness. For aluminium inoculated with Al–Ti–B, zirconium in particular has a strong poisoning effect. This appears to be attributable mainly to hindrance of nucleation, by substitution of Zr for Ti in the TiB_2 particles or in their Al_3Ti coating [28]. Also, different batches of nominally identical refiner can behave differently. An anomalous sample of refiner with poor performance was found to give a grain diameter four times that for a standard refiner under the same conditions. The difference in performance could not be explained by the free-growth model, as poor and standard refiners had essentially the same particle-diameter distribution [3]. On the other hand, holding the poor refiner in the melt, improved its performance to that of a standard good refiner [27]. This improvement has been attributed to the development of a suitable Al_3Ti layer on the borides.

Especially for lower refiner addition levels, lower solute levels, and lower cooling rates, some experiments yielded columnar or only partially refined structures. The model treats only equiaxed growth and may therefore make unrealistic predictions outside the limits of its applicability. To describe different types of casting and variations in casting conditions, the only input parameter in the present model is the cooling rate. This is inadequate, especially in the presence of steep temperature gradients, for which columnar growth would dominate. However, extension of the modelling to the analysis of the columnar-to-equiaxed transition is beyond the scope of the present work. The transition is affected by the temperature gradient, completely ignored in the present modelling. Temperature-gradient effects, including the columnar-to-equiaxed transition, have been treated using microstructural modelling, such as cellular-automaton, finite-element modelling [40]. Similar modelling is now being applied to understand grain refinement when there are significant temperature gradients in the melt [41].

The present model does not include dendritic growth and this precludes detailed calculation of recalescence. The prediction of cooling curves is further hindered by temperature gradients in the solidifying sample. Measured cooling curves would be an ideal test of the modelling, and provide a possible diagnostic in practice. A complete fitting, taking account of the overall microstructural development in a sample, would be very worthwhile.

Full prediction of as-cast grain structure may require inclusion also of fluid-flow effects and dendrite fragmentation. Finally, even the as-cast structure may in principle be affected by solid-state processes such as grain growth occurring during cooling. Such processes have not been accounted for, and they are unlikely to be significant.

8. CONCLUSIONS

A model has been developed for the prediction of as-cast grain size in inoculated melts. This adapts an earlier model of Maxwell and Hellawell [2] by taking the appearance of grains to be controlled by the condition for free growth rather than by nucleation, and by taking a distribution of inoculant particle diameters. The number of grains is limited by recalescence of the melt. Without adjustable parameters, the model fits quantitatively the measured grain size in standard (TP-1) tests on commercial purity and other aluminium alloys inoculated with an Al–Ti–B refiner. The variations of grain size with refiner addition level, cooling rate and alloy composition are all adequately modelled. This suggests that nucleation on the TiB_2 particles in the refiner occurs at very low undercooling, possibly by an adsorption mechanism. The model breaks down in the presence of columnar growth, and when nucleation on the inoculant particles is impaired, for example by poisoning. According to the model, the effectiveness of a refiner may be optimized at a particular average particle diameter.

That quantitative predictions can be made for the number of effective nucleation events in solidification is unusual; this is possible in the present case because grain initiation is dominated by added inoculant particles of high nucleation potency.

Acknowledgements—A.M.B. is grateful to the Engineering and Physical Sciences Research Council and to the London and Scandinavian Metallurgical Co. Limited (LSM) for a CASE Studentship in support of this work. A.T. acknowledges the support of a CIFRE studentship supported by Pechiney CRV and by LSM. Professor A. H. Windle is thanked for provision of laboratory facilities. The authors acknowledge the assistance of Mr M. Riaz (LSM) with the grain-refining tests. Thanks are due to Professor A. Hellawell (Michigan Technological University), Dr Ph. Jarry (Pechiney CRV), Dr M. A. Kearns (LSM) and Dr P. Schumacher (University of Oxford) for useful discussions.

REFERENCES

1. McCartney, D. G., *Int. Mater. Rev.*, 1989, **34**, 247.
2. Maxwell, I. and Hellawell, A., *Acta metall.*, 1975, **23**, 229.
3. Bunn, A. M., Evans, P. V., Bristow, D. J. and Greer, A. L., in *Light Metals*, ed. B. Welch. TMS, Warrendale, PA, 1998, pp. 963–968.
4. Arnberg, L., Bäckerud, L. and Klang, H., *Metals Technol.*, 1982, **9**, 1.
5. Clyne, T. W. and Robert, M. H., *Metals Technol.*, 1980, **7**, 177.
6. Pearson, J., Birch, M. E. J. and Hadlet, D., in *Proc. Conf. Solidification Technology in the Foundry and Casthouse*. The Metals Society, London, 1983, p. 74.
7. Schumacher, P. and Greer, A. L., *Mater. Sci. Engng A*, 1994, **A178**, 309.

8. Schumacher, P. and Greer, A. L., *Mater. Sci. Engng A*, 1994, **A181/A182**, 1335.
9. Schumacher, P. and Greer, A. L., in *Light Metals*, ed. J. W. Evans. TMS, Warrendale, PA, 1995, pp. 869–877.
10. Schumacher, P. and Greer, A. L., in *Light Metals*, ed. W. Hale. TMS, Warrendale, PA, 1996, pp. 745–753.
11. Schumacher, P., Greer, A. L., Worth, J., Evans, P. V., Kearns, M. A., Fisher, P. and Green, A. H., *Mater. Sci. Technol.*, 1998, **14**, 394.
12. Marcantonio, J. A. and Mondolfo, L. F., *Metall. Trans.*, 1971, **2**, 465.
13. Kim, W. T., Zhang, D. L. and Cantor, B., *Metall. Trans. A*, 1991, **22**, 2487.
14. Kim, W. T. and Cantor, B., *Acta metall. mater.*, 1994, **42**, 3045.
15. Kim, W. T. and Cantor, B., *Acta metall. mater.*, 1994, **42**, 3115.
16. O'Reilly, K. A. Q. and Cantor, B., *Acta metall.*, 1995, **43**, 405.
17. Guzowski, M. M., Sigworth, G. K. and Sentner, D. A., *Metall. Trans. A*, 1987, **18**, 603.
18. Bäckerud, L. and Yidong, S., *Aluminium*, 1991, **67**, 780.
19. Johnsson, M., Bäckerud, L. and Sigworth, G. K., *Metall. Trans. A*, 1993, **24**, 481.
20. Tarshis, C. A., Walker, J. L. and Rutter, J. W., *Metall. Trans.*, 1971, **2**, 2589.
21. Johnsson, M., *Z. Metallk.*, 1994, **85**, 781.
22. Kearns, M. A. and Cooper, P. S., *Mater. Sci. Technol.*, 1997, **13**, 650.
23. Desnain, P., Fautrelle, Y., Meyer, J.-L., Riquet, J.-P. and Durand, F., *Acta metall. mater.*, 1990, **38**, 1513.
24. Hodaj, F. and Durand, F., *Acta mater.*, 1997, **45**, 2121.
25. Spittle, J. A. and Sadli, S. B., *Mater. Sci. Technol.*, 1995, **11**, 533.
26. *Standard Test Procedure for Aluminum Alloy Grain Refiners: TP-1*. The Aluminum Association, Washington, DC, 1987.
27. Bunn, A. M., Greer, A. L., Green, A. H. and Kearns, M. A., in *Solidification Processing 1997*, ed. J. Beech and H. Jones. The University of Sheffield, Sheffield, 1997, pp. 264–267.
28. Bunn, A. M., Schumacher, P., Kearns, M. A., Boothroyd, C. B. and Greer, A. L., *Mater. Sci. Technol.*, 1999, **15**, 1115.
29. Mueller, B. A. and Perepezko, J. H., *Metall. Trans. A*, 1987, **18A**, 1143.
30. Eustathopoulos, N., Coudurier, L., Joud, J. C. and Desré, P., *J. Cryst. Growth*, 1976, **33**, 105.
31. Brandes, E. A. (ed.), *Smithells Metals Reference Book*, 6th edn. Butterworths, London, 1983, pp. 8-1–14-1.
32. Kurz, W. and Fisher, D. J., *Fundamentals of Solidification*, 3rd edn. Trans Tech. Publications, Switzerland, 1992.
33. Eremenko, V. N., Natanzon, V. N. and Titov, V. P., *Fizika Khim. Mekh. Mater.*, 1978, **14**, 3.
34. Aaron, H. B., Fainstein, D. and Kotler, G. R., *J. appl. Phys.*, 1970, **41**, 4405.
35. Mullins, W. W. and Sekerka, R. F., *J. appl. Phys.*, 1963, **34**, 323.
36. Massalski, T. B. (ed.), *Binary Alloy Phase Diagrams*, Vol. 1, 2nd edn. ASM International, Materials Park, 1990.
37. Underwood, E. E., *Quantitative Stereology*. Addison-Wesley, Reading, MA, 1970.
38. Spittle, J. A. and Brown, S. G. R., *Acta metall.*, 1989, **37**, 1803.
39. Tronche, A. and Greer, A. L., in *Light Metals 2000*, ed. R. D. Peterson. TMS, Warrendale, PA, 2000, pp. 827–832.
40. Gandin, Ch.-A. and Rappaz, M., *Acta metall. mater.*, 1994, **42**, 2233.
41. Greer, A. L., Tronche, A. and Vandyoussefi, M., *Mater. Res. Soc. Symp. Proc.*, 2000, **578**.
42. Smith, C. S., *Trans. Am. Soc. Metals*, 1953, **45**, 533.
43. Mendelson, M. I., *J. Am. Ceram. Soc.*, 1969, **52**, 443.
44. Feltham, P., *Acta metall.*, 1957, **5**, 97.
45. Herdan, G., in *Small Particle Statistics*. Butterworths, London, 1960, p. 83.

APPENDIX

The relationship between mean linear intercept and number of grains per unit volume

Throughout the present work, the grain diameter is quoted as the mean linear intercept $\bar{l}$. The fundamental quantity calculated by the model is the number of grains per unit volume of sample N_V. The relationship between N_V and $\bar{l}$ is not straightforward, and indeed depends on the grain-size distribution which has not been determined. An approximate relationship is derived, assuming an equiaxed grain structure with a grain-size distribution typical of a metal.

The grain shape is taken to be the tetrakaidecahedron [42]. The size of a grain can be described by its calliper diameter D, defined as the mean perpendicular distance, averaged over all orientations, between two parallel tangent planes on the tetrakaidecahedron [43]. It is assumed that the real grain structure has a range of values of D, *log-normally* distributed. The geometric-mean value $\bar{D}_g$ is then related to the mean linear intercept in this case by

$$\bar{D}_g = 1.7756 \exp[-2.5(\ln \sigma)^2]\bar{l} \qquad \text{(A1)}$$

where $\ln \sigma$ is the standard deviation of the log-normal distribution [43]. As discussed in Ref. [44], the grain-size distribution for a metallic microstructure undergoing grain growth is indeed log-normal, typically with $\ln \sigma = 0.23$. We assume, without specific justification, that such a distribution will also be a reasonable description for a refined, as-solidified grain structure. Substituting $\ln \sigma = 0.23$ in equation (A1) gives

$$\bar{D}_g = 1.558\bar{l}. \qquad \text{(A2)}$$

The simple arithmetic mean $\bar{D}$ of a log-normal distribution is given by [45]

$$\bar{D} = \bar{D}_g \exp[0.5(\ln \sigma)^2] = 1.027\bar{D}_g \qquad \text{(A3)}$$

with the assumed value of $\ln \sigma$. Furthermore the volume-weighted arithmetic mean $\bar{D}_V$ is given by [45]

$$\bar{D}_V = \bar{D} \exp[(\ln \sigma)^2] = 1.054\bar{D} \qquad \text{(A4)}$$

again taking $\ln \sigma = 0.23$. Combining equations (A2)–(A4), we have

$$\bar{D}_V = 1.686\bar{l}. \tag{A5}$$

From the expression for the volume of a tetrakaidecahedron in terms of its calliper diameter [43], it follows that for a grain-size distribution described by $\bar{D}_V$, N_V the number of grains per unit volume is given by

$$N_V = \frac{27}{8\sqrt{2}\bar{D}_V^3} = \frac{2.386}{\bar{D}_V^3}. \tag{A6}$$

Substituting from equation (A5), we obtain the relationship which is used throughout the present work:

$$N_V = \frac{0.5}{\bar{l}^3}. \tag{A7}$$